Computers & Fluids Vol. 17, No. 1, pp. 135–150, 1989
Printed in Great Britain.

0045-7930/89 $3.00 + 0.00

THE SOLUTION OF THE NAVIER–STOKES EQUATIONS USING GAUSS–SEIDEL LINE RELAXATION

ROBERT W. MACCORMACK and GRAHAM V. CANDLER
Stanford University, Department of Aeronautics and Astronautics, Stanford, CA 94305, U.S.A.

(*Received* 18 *September* 1987; *received for publication* 10 *March* 1988)

Abstract—Gauss–Seidel line relaxation is used to solve an implicit flux split difference approximation to the Navier–Stokes equations. The flux split approximation is chosen to maximize the weight of the diagonal elements of the block matrix elements that need to be inverted iteratively by the Gauss–Seidel procedure. There are several flux split approximations that can be chosen. However, not all are suitable for viscous flows containing shear or boundary layers. The present paper will illustrate the adverse effects of flux splitting in viscous flow calculations and propose corrections. The numerical procedures will be applied to solve for subsonic laminar flow past a flat plate, turbulent flow past a cone at Mach 6, and chemical and thermal nonequilibrium flow past a sphere-cone body at Mach 18.

INTRODUCTION

There are many papers [1–4] that have appeared in recent years that use Gauss–Seidel line relaxation to numerically solve the Navier–Stokes equations. This method avoids the numerical inefficiency of using approximately factored procedures that have been the workhorse of compressible viscous computational fluid dynamics during the past decade. However, to enhance the numerical convergence of the unfactored procedure, the weights of the diagonal matrix elements appearing in the difference equations that approximate the governing flow equations are increased by using flux split, or upwind, difference approximations. The flux split procedures, largely developed by Steger and Warming [5], were introduced primarily to solve the equations governing inviscid flow. At present, there is still considerable uncertainty on their ability to calculate viscous shear or boundary layer flow [6].

The flux split procedures are flow type dependent procedures that choose forward, backward, and central difference approximations to flow derivatives according to local domain of dependence considerations. Perhaps the first such finite difference procedure for mixed flows was presented by Vincenti, Wagoner and Fisher in 1956 [7], for transonic flow past an inclined flat plate. They solved the governing equations in the hodograph plane and had 8 different categories of mesh points depending on whether they were regular subsonic points, regular supersonic points, or were located adjacent to sonic lines, shock waves, stagnation points etc. In the early 1970's Murman and Cole [8] used both type dependent differencing and Gauss–Seidel line relaxation to solve the Transonic Small Disturbance equation directly in the physical plane. Jameson [9] soon followed using these same two key ingredients plus a local coordinate rotation to solve the Full Potential equation.

Type dependent differencing of the Euler equations was introduced by Moretti [10] in the mid-1970's within his "Lambda" scheme for solving the gas dynamic equations in nonconservation law form. Steger and Warming in their "Flux Vector Splitting" procedure applied type dependent differencing directly to the governing equations in conservation law form. These advances significantly improved the numerical resolution of the hyperbolic features of the flow. Additionally, their formulation increased the weights of the diagonal elements in the block matrix representation of the difference equations used to approximate the governing flow equations. This latter feature made practical the iterative inversion of implicit block matrix formulations of the governing equations by Gauss–Seidel line relaxation. Previously, the block matrix equation had to be factored into block tridiagonal elements for sequential direct inversion. Unfortunately, the factoring was only approximate and it introduced error that severely limited the time step size, causing slow numerical convergence histories. The Gauss–Seidel line relaxation of the unfactored equations is not so limited and for large time step choices it approaches a rapidly converging Newton procedure.

A decade and a half after the landmark papers of Murman–Cole and Jameson for solving the potential equations, Chakravarthy [11] applied type dependent differencing and Gauss–Seidel line relaxation to solve the Euler equations. And, as previously stated, there have been several recent applications using this approach to solve the Navier–Stokes equations. Yet, some uncertainty on the validity of using flux split procedures to calculate viscous phenomena still exists.

There are several different ways to apply flux vector splitting [6]. Unfortunately, many of them are unsuitable for solving viscous flow problems containing shear or boundary layers. The difficulty with flux splitting arises in two ways, either an abnormally large numerical mixing of the fluid occurs within the boundary layer, or a fictitious pressure gradient is created that causes an unrealistic convection within the layer. This paper will analyze these difficulties, propose remedies for their removal, and attempt to demonstrate that accurate skin friction and heat transfer values can be obtained by applying the revised flux split procedures to calculate the subsonic laminar flow past a flat plate and the supersonic turbulent flow past a cone at Mach 6. In addition, some recently obtained results for hypersonic flow past a sphere cone-body by a chemically reacting gas in thermal nonequilibrium will be presented to demonstrate the power of these procedures.

FLUX VECTOR SPLITTING

We can write the Navier–Stokes equations in the following 2-D form:

$$\frac{\partial U}{\partial t}+\frac{\partial F}{\partial x}+\frac{\partial G}{\partial y}+\text{viscous terms}=0$$

where

$$U=\begin{bmatrix}\rho\\ \rho u\\ \rho v\\ e\end{bmatrix},\qquad F=\begin{bmatrix}\rho u\\ \rho u^2+p\\ \rho vu\\ (e+p)u\end{bmatrix},\quad\text{and}\quad G=\begin{bmatrix}\rho v\\ \rho uv\\ \rho v^2+p\\ (e+p)v\end{bmatrix},$$

$$p=(\gamma-1)\rho\epsilon\qquad\text{and}\qquad \epsilon=e/\rho-\tfrac{1}{2}(u^2+v^2)$$

The vector equation above is written in terms of density ρ, Cartesian velocities u and v, pressure p, and total energy per unit volume e. The equation can be transformed for use in a general coordinate system (see Fig. 1) as follows.

$$\frac{\partial U'}{\partial t}+\frac{\partial F'}{\partial \xi}+\frac{\partial G'}{\partial \eta}+\text{viscous terms}=0, \tag{1}$$

where:

$$U'=UJ,\qquad F'=\left(F\frac{\partial \xi}{\partial x}+G\frac{\partial \xi}{\partial y}+U\frac{\partial \xi}{\partial t}\right)J,$$

$$G'=\left(F\frac{\partial \eta}{\partial x}+G\frac{\partial \eta}{\partial y}+U\frac{\partial \eta}{\partial t}\right)J,\quad\text{and}\quad J=\left(\frac{\partial \xi}{\partial x}\frac{\partial \eta}{\partial y}-\frac{\partial \xi}{\partial y}\frac{\partial \eta}{\partial x}\right)^{-1}.$$

Using the identities:

$$\frac{\partial x}{\partial \xi}=\frac{\partial \eta}{\partial y}J,\qquad \frac{\partial y}{\partial \xi}=-\frac{\partial \eta}{\partial x}J,\qquad \frac{\partial x}{\partial \eta}=-\frac{\partial \xi}{\partial y}J,\qquad \frac{\partial y}{\partial \eta}=\frac{\partial \xi}{\partial x}J,\quad\text{and}\quad J=V=\frac{\partial x}{\partial \xi}\frac{\partial y}{\partial \eta}-\frac{\partial x}{\partial \eta}\frac{\partial y}{\partial \xi},$$

and assuming that the general coordinate system is stationary with respect to the original Cartesian system, we can write the general, or rotated, flux vectors as:

$$F'=\frac{\partial y}{\partial \eta}F-\frac{\partial x}{\partial \eta}G\quad\text{and}\quad G'=-\frac{\partial y}{\partial \xi}F+\frac{\partial x}{\partial \xi}G. \tag{2}$$

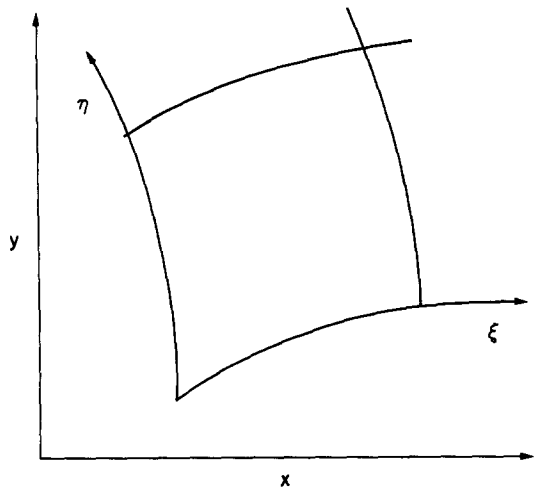

Fig. 1. Cartesian and general coordinate systems.

We can represent the rotated flux vectors each as the product of a rotated Jacobian matrix and the solution vector U.

$$F' = A'U \quad \text{and} \quad G' = B'U$$

where

$$A' = \frac{\partial y}{\partial \eta} A - \frac{\partial x}{\partial \eta} B, \qquad B' = -\frac{\partial y}{\partial \xi} A + \frac{\partial x}{\partial \xi} B, \qquad A = \frac{\partial F}{\partial U}, \quad \text{and} \quad B = \frac{\partial G}{\partial U}.$$

The rotated Jacobians can be diagonalized as follows

$$A' = S^{-1} R_{A'}^{-1} C_{A'}^{-1} \Lambda_{A'} C_{A'} R_{A'} S, \qquad B' = S^{-1} R_{B'}^{-1} C_{B'}^{-1} \Lambda_{B'} C_{B'} R_{B'} S,$$

where

$$S = \begin{bmatrix} 1 & 0 & 0 & 0 \\ -u/\rho & 1/\rho & 0 & 0 \\ -v/\rho & 0 & 1/\rho & 0 \\ \alpha\beta & -u\beta & -v\beta & \beta \end{bmatrix},$$

$$R_{A'} = \frac{1}{d_{A'}} \begin{bmatrix} d_{A'} & 0 & 0 & 0 \\ 0 & \dfrac{\partial y}{\partial \eta} & -\dfrac{\partial x}{\partial \eta} & 0 \\ 0 & \dfrac{\partial x}{\partial \eta} & \dfrac{\partial y}{\partial \eta} & 0 \\ 0 & 0 & 0 & d_{A'} \end{bmatrix}, \qquad R_{B'} = \frac{1}{d_{B'}} \begin{bmatrix} d_{B'} & 0 & 0 & 0 \\ 0 & \dfrac{\partial x}{\partial \xi} & \dfrac{\partial y}{\partial \xi} & 0 \\ 0 & -\dfrac{\partial y}{\partial \xi} & \dfrac{\partial x}{\partial \xi} & 0 \\ 0 & 0 & 0 & d_{B'} \end{bmatrix},$$

$$C_{A'} = \begin{bmatrix} 1 & 0 & 0 & -1/c^2 \\ 0 & \rho c & 0 & 0 \\ 0 & 0 & 1 & 0 \\ 0 & -\rho c & 0 & 0 \end{bmatrix}, \qquad C_{B'} = \begin{bmatrix} 1 & 0 & 0 & -1/c^2 \\ 0 & 1 & 0 & 0 \\ 0 & 0 & \rho c & 1 \\ 0 & 0 & -\rho c & 1 \end{bmatrix},$$

$$\Lambda_{A'} = d_{A'} \begin{bmatrix} u' & 0 & 0 & 0 \\ 0 & u'+c & 0 & 0 \\ 0 & 0 & u' & 0 \\ 0 & 0 & 0 & u'-c \end{bmatrix}, \qquad \Lambda_{B'} = d_{B'} \begin{bmatrix} v' & 0 & 0 & 0 \\ 0 & v' & 0 & 0 \\ 0 & 0 & v'+c & 0 \\ 0 & 0 & 0 & v'-c \end{bmatrix},$$

where

$$\alpha = \tfrac{1}{2}(u^2 + v^2), \qquad \beta = \gamma - 1,$$

$$c = \sqrt{\gamma p/\rho}, \qquad d_{A'} = \sqrt{\left(\frac{\partial x}{\partial \eta}\right)^2 + \left(\frac{\partial y}{\partial \eta}\right)^2},$$

$$d_{B'} = \sqrt{\left(\frac{\partial x}{\partial \xi}\right)^2 + \left(\frac{\partial y}{\partial \xi}\right)^2}, \qquad u' = \left(\frac{\partial y}{\partial \eta}\, u - \frac{\partial x}{\partial \eta}\, v\right) \Big/ d_{A'},$$

and

$$v' = \left(-\frac{\partial y}{\partial \xi}\, u + \frac{\partial x}{\partial \xi}\, v\right) \Big/ d_{B'}.$$

The matrices $R_{A'}$ and $R_{B'}$ represent rotation matrices and u' and v' are rotated velocity vectors. The rotated Jacobian matrices A' and B' can be split into positive and negative parts.

$$A'_+ = S^{-1} R_{A'}^{-1} C_{A'}^{-1} \Lambda_{+_{A'}} C_{A'} R_{A'} S, \qquad A'_- = S^{-1} R_{A'}^{-1} C_{A'}^{-1} \Lambda_{-_{A'}} C_{A'} R_{A'} S,$$

$$B'_+ = S^{-1} R_{B'}^{-1} C_{B'}^{-1} \Lambda_{+_{B'}} C_{B'} R_{B'} S, \qquad B'_- = S^{-1} R_{B'}^{-1} C_{B'}^{-1} \Lambda_{-_{B'}} C_{B'} R_{B'} S,$$

where Λ_+ or Λ_- designate diagonal matrices containing only the positive or negative elements, respectively, of the diagonal matrix Λ.

Split fluxes can be defined by:

$$F'_+ = A'_+ U, \qquad F'_- = A'_- U, \qquad G'_+ = B'_+ U, \qquad G'_- = B'_- U$$

Note $F' = F'_+ + F'_-$ and $G' = G'_+ + G'_-$.

Equation (1) can now be rewritten as:

$$\frac{\partial U}{\partial t} + \frac{1}{V}\left(\frac{\partial F'_+}{\partial \xi} + \frac{\partial F'_-}{\partial \xi} + \frac{\partial G'_+}{\partial \eta} + \frac{\partial G'_-}{\partial \eta} + \text{viscous terms}\right) = 0.$$

A first order accurate explicit finite difference equation, according to Steger and Warming [5] and neglecting for the moment the numerical treatment of the viscous terms, is

$$U_{i,j}^{n+1} = U_{i,j}^n - \frac{\Delta t}{V_{i,j}}\left(\frac{D_-}{\Delta \xi} \cdot F'_+ + \frac{D_+}{\Delta \xi} \cdot F'_- + \frac{D_-}{\Delta \eta} \cdot G'_+ + \frac{D_+}{\Delta \eta} \cdot G'_- + \text{viscous terms}\right)^n_{i,j}$$

where

$$\frac{D_+}{\Delta \xi}, \qquad \frac{D_-}{\Delta \xi}, \qquad \frac{D_+}{\Delta \eta}, \quad \text{and} \quad \frac{D_-}{\Delta \eta}$$

represent first order accurate and backward difference operators in the ξ and η coordinate directions, respectively.

We can write the above difference equation in conservation law like form as:

$$U_{i,j}^{n+1} = U_{i,j}^n - \frac{\Delta t}{V_{i,j}}\left(\frac{F'_{i+1/2,j} - F'_{i-1/2,j}}{\Delta \xi} + \frac{G'_{i,j+1/2} - G'_{i,j-1/2}}{\Delta \eta} + \text{viscous terms}\right), \tag{3}$$

where

$$F'_{i+1/2,j} = A'_{+_{i,j}} U_{i,j}^n + A'_{-_{i+i,j}} U_{i+i,j}^n \quad \text{and} \quad G'_{i,j+1/2} = B'_{+_{i,j}} U_{i,j}^n + B'_{-_{i,j+1}} U_{i,j+1}^n \tag{4}$$

The above split flux definitions will be referred to as the Steger–Warming split flux.

FLUX SPLITTING IN BOUNDARY LAYERS

We are going to demonstrate that the above Steger–Warming split flux definition, eqn (4), is inappropriate for viscous shear layer problems because it introduces into the calculation an unacceptably large numerical diffusion. In fairness, the flux split procedure was introduced to solve the inviscid equations of fluid flow. It is ironic that where it is needed least, in viscous dominated regions of the flow, it can strongly adversely influence the accuracy of the calculation. We will propose some simple modifications that will improve significantly the accuracy of shear layer

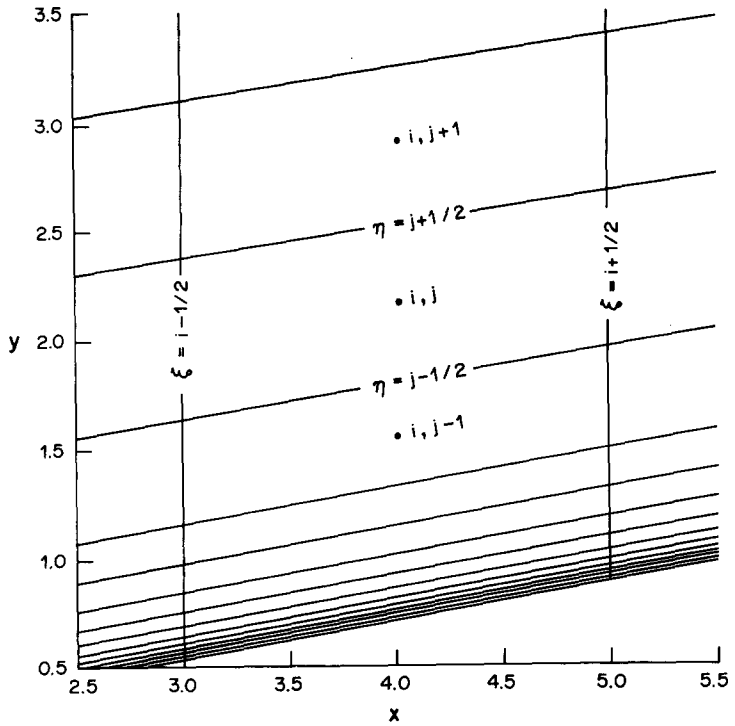

Fig. 2. Boundary layer mesh.

calculations. We start by considering the rotated flux vector G' at surface $j + 1/2$ in Fig. 2. Note for convenience we have chosen our general coordinates ξ and η so that they have integer values at mesh points, located at cell centers, and half integer values at mesh lines. The mesh lines form the cell surfaces surrounding the mesh points. Thus, $\Delta\xi = \Delta\eta = 1$, and $V_{i,j}$ represents cell volume. The above difference eqn (3) can be thought of equally as either a finite difference or finite volume equation. The flux vector $G'_{i,j+1/2}$ should approximate the following vector [see eqn (2)] at $\xi = i$, $\eta = j + 1/2$.

$$G' = d_{B'} \begin{bmatrix} \rho v' \\ \rho u v' - \dfrac{1}{d_{B'}} \dfrac{\partial y}{\partial \xi} p \\ \rho v v' + \dfrac{1}{d_{B'}} \dfrac{\partial x}{\partial \xi} p \\ (e + p) v' \end{bmatrix}. \tag{5}$$

(a) Excessive numerical dissipation

Now let's examine the split flux approximation by direct though lengthy calculation under boundary layer conditions. The flux split procedures act on only the hyperbolic, or inviscid, terms of the governing equations. The parabolic, or viscous, terms are treated by other procedures. The boundary layer is fairly benign from the hyperbolic point of view. Pressure gradients and convection velocities across the layer are small. This region, whose principal feature is the tangential velocity gradient, essentially consists of fluid layers sliding relative to one another. For algebraic simplicity, let's assume that in the neighborhood of boundary layer point (i, j)

(1) p, c, and v' are constant,
(2) u' varies from 0 at the wall to u'_e at the boundary layer edge.
(3) v' is positive and negligibly small compared to u'_e or c.

In the split flux approximation (dropping the subscript B' for convenience)

$$G'_{\pm} = B'_{\pm} U = S^{-1} R^{-1} C^{-1} \Lambda_{\pm} CRSU$$

$$= S^{-1} R^{-1} C^{-1} \Lambda_{\pm} CR \begin{bmatrix} 1 & 0 & 0 & 0 \\ -u/\rho & 1/\rho & 0 & 0 \\ -v/\rho & 0 & 1/\rho & 0 \\ \alpha\beta & -u\beta & -v\beta & \beta \end{bmatrix} \begin{bmatrix} \rho \\ \rho u \\ \rho v \\ e \end{bmatrix},$$

$$= S^{-1} R^{-1} C^{-1} \Lambda_{\pm} C \frac{1}{d_{B'}} \begin{bmatrix} d_{B'} & 0 & 0 & 0 \\ 0 & \dfrac{\partial x}{\partial \xi} & \dfrac{\partial y}{\partial \xi} & 0 \\ 0 & -\dfrac{\partial y}{\partial \xi} & \dfrac{\partial x}{\partial \xi} & 0 \\ 0 & 0 & 0 & d_{B'} \end{bmatrix} \begin{bmatrix} \rho \\ 0 \\ 0 \\ p \end{bmatrix}.$$

Note the surprising result that all that remains of the original U vector after our first matrix multiplication is density and pressure. All information about the velocity field is entirely lost. Continuing our evaluation,

$$G'_{\pm} = S^{-1} R^{-1} C^{-1} \Lambda_{\pm} \begin{bmatrix} 1 & 0 & 0 & -1/c^2 \\ 0 & 1 & 0 & 0 \\ 0 & 0 & \rho c & 1 \\ 0 & 0 & -\rho c & 1 \end{bmatrix} \begin{bmatrix} \rho \\ 0 \\ 0 \\ p \end{bmatrix} = S^{-1} R^{-1} C^{-1} \Lambda_{\pm} \begin{bmatrix} \rho - p/c^2 \\ 0 \\ p \\ p \end{bmatrix}.$$

Now, $\lambda_4 = v' - c < 0$, $G'_{-} = G'_{\lambda_4}$

$$G'_{\lambda_4} = S^{-1} R^{-1} C^{-1} d_{B'} \begin{bmatrix} 0 & 0 & 0 & 0 \\ 0 & 0 & 0 & 0 \\ 0 & 0 & 0 & 0 \\ 0 & 0 & 0 & \lambda_4 \end{bmatrix} \begin{bmatrix} \rho - p/c^2 \\ 0 \\ p \\ p \end{bmatrix}_{i,j+1}$$

$$= S^{-1} R^{-1} d_{B'} \begin{bmatrix} 1 & 0 & \dfrac{1}{2c^2} & \dfrac{1}{2c^2} \\ 0 & 1 & 0 & 0 \\ 0 & 0 & \dfrac{1}{2\rho c} & \dfrac{-1}{2\rho c} \\ 0 & 0 & 1/2 & 1/2 \end{bmatrix} \begin{bmatrix} 0 \\ 0 \\ 0 \\ \lambda_4 p \end{bmatrix}_{i,j+1}$$

$$= S^{-1} \begin{bmatrix} d_{B'} & 0 & 0 & 0 \\ 0 & \dfrac{\partial x}{\partial \xi} & -\dfrac{\partial y}{\partial \xi} & 0 \\ 0 & \dfrac{\partial y}{\partial \xi} & \dfrac{\partial x}{\partial \xi} & 0 \\ 0 & 0 & 0 & d_{B'} \end{bmatrix} \begin{bmatrix} \lambda_4 p/2c^2 \\ 0 \\ -\lambda_4 p/2\rho c \\ \lambda_4 p/2 \end{bmatrix}_{i,j+1}$$

$$= \begin{bmatrix} 1 & 0 & 0 & 0 \\ u & \rho & 0 & 0 \\ v & 0 & \rho & 0 \\ \alpha & \rho u & \rho v & 1/\beta \end{bmatrix} \begin{bmatrix} d_{B'} \lambda_4 p/c^2 \\ \dfrac{\partial y}{\partial \xi} \lambda_4 p/2\rho c \\ -\dfrac{\partial x}{\partial \xi} \lambda_4 p/2\rho c \\ d_{B'} \lambda_4 p/2 \end{bmatrix}_{i,j+1},$$

or

$$G'_{\lambda_4} = \begin{bmatrix} 1/2c^2 \\ u/2c^2 + \dfrac{\partial y}{\partial \xi}\Big/ 2cd_{B'} \\ v/2c^2 - \dfrac{\partial x}{\partial \xi}\Big/ 2cd_{B'} \\ \alpha/2c^2 - v'/2c + 1/2\beta \end{bmatrix}_{i,j+1} d_{B'}(v' - c)p_{i,j+1}.$$

Similarly, with $\lambda_1 = v'$ and $\lambda_3 = v' + c$:

$$G'_{\lambda_1} = \begin{bmatrix} 1 \\ u \\ v \\ \alpha \end{bmatrix}_{i,j} d_{B'}v'(\rho_{i,j} - p_{i,j}/c^2)$$

and

$$G'_{\lambda_3} = \begin{bmatrix} 1/2c^2 \\ u/2c^2 - \dfrac{\partial y}{\partial \xi}\Big/ 2cd_{B'} \\ v/2c^2 + \dfrac{\partial x}{\partial \xi}\Big/ 2cd_{B'} \\ \alpha/2c^2 + v'/2c + 1/2\beta \end{bmatrix}_{i,j} d_{B'}(v' + c)p_{i,j}.$$

$$G'_{i,j+1/2} = G'_{\lambda_1} + G'_{\lambda_2} + G'_{\lambda_3}$$

If we examine the first element of the vector $G'_{i,j+1/2}$ we obtain using assumption (1):

$$g_1 = d_{B'}\left[v'\left(\rho_{i,j} - \frac{p_{i,j}}{c^2}\right) + \frac{1}{2c^2}\left((v' + c)p_{i,j} + (v' - c)p_{i,j+1}\right)\right] \simeq d_{B'}\rho_{i,j}v',$$

which is indeed a valid approximation to the first element of G' given in eqn (5). Note that this approximation was achieved by the counter balancing of two large terms of magnitude $c(p/2c^2) = c/(2\gamma)\rho$. That is, there was an equal exchange of mass per unit volume at a whopping convection speed of $c/2\gamma$ between cell (i, j) and cell $(i, j + 1)$ that resulted in no net mass transfer. However, if we now examine the second element of the vector $G'_{i,j+1/2}$

$$\begin{aligned} g_2 = d_{B'}\Bigg[& v'\left(\rho_{i,j} - \frac{p_{i,j}}{c^2}\right)u_{i,j} + \frac{1}{2c^2}\left((v' + c)p_{i,j}u_{i,j} + (v' - c)p_{i,j+1}u_{i,j+1}\right) \\ & + \frac{\partial y}{\partial \xi}\frac{1}{2cd_{B'}}\left(-(v' + c)p_{i,j} + (v' - c)p_{i,j+1}\right)\Bigg] \\ \simeq d_{B'}\Bigg[& \rho_{i,j}u_{i,j}v' - \frac{1}{d_{B'}}\frac{\partial y}{\partial \xi}p + \frac{c}{2\gamma}\rho_{i,j}(u_{i,j+1} - u_{i,j})\Bigg]. \end{aligned}$$

The first two terms on the right above approximate the second element of G' given in eqn (5), but the third term represents a significant exchange, or mixing, of tangential momentum between cells (i, j) and $(i, j + 1)$. Under our boundary layer assumptions, the gradient of tangential velocity is nonzero and, unlike the case of the first element of the flux vector, there results a significant tangential momentum exchange. This mixing, caused solely by the flux splitting of the inviscid flux terms is purely numerical and, although it is of order Δy, it can dwarf the true physical mixing represented by the viscous terms. Similarly, there is also an unacceptably large numerical exchange of kinetic energy of the order of, $d_{B'}(c/2\gamma)\rho_{i,j}(\alpha_{i,j+1} - \alpha_{i,j})$, between adjacent points within the boundary layer.

The excessive numerical diffusion is caused by the choice of indices occurring on the split Jacobians defining the Steger–Warming flux split approximation to G' in eqn (4). If we trace through the derivation once more, it is seen in particular that the mixing is caused by the difference in indices appearing on the S^{-1} matrix factor of the split Jacobians B'_- and B'_+. If instead the split flux formulas were given by:

$$F'_{i+1/2,j} = A'_{+_{i+1/2,j}} U^n_{i,j} + A'_{-_{i+1/2,j}} U^n_{i+1,j} \quad \text{and} \quad G'_{i,j+1/2} = B'_{+_{i,j+1/2}} U^n_{i,j} + B'_{-_{i,j+1/2}} U^n_{i,j+1} \tag{6}$$

where the A'_+ and A'_-, and the B'_+ and B'_- matrices are defined using the same flow variables respectively, a cancellation, similar to that for the first element g_1, would occur for all elements, thus, preventing excessive numerical mixing.

In the present study the half integer indices $i + 1/2$ or $j + 1/2$ alternate between i and $i + 1$ or j and $j + 1$, respectively. For example:

$$j + 1/2 = \begin{cases} j, & n \text{ odd} \\ j+1, & n \text{ even} \end{cases}.$$

Alternatively, the half integer values could indicate that the flow variables used for split Jacobians are averaged from those at points i and $i + 1$ or j and $j + 1$, respectively.

Both flux split procedures of eqns (4) and (6) were used to calculate the flow plate at Mach 0.6. This test case was chosen because we can compare our results directly with the exact Blasius solution. The calculated boundary layer velocity profiles at $\mathrm{Re}_x = 4.6 \times 10^6$ are compared to the Blasius solution in Fig. 3. The Steger–Warming form of flux splitting results in excessive numerical mixing throughout the boundary layer as predicted. The modified form of flux splitting of eqn (6) is significantly better. However, it also shows unacceptable errors close to the wall and near the "knee" of the profile.

(b) Fictitious pressure gradients

Defining both B'_+ and B'_- from the same values of the dependent flow variables significantly improved the calculation of boundary layer velocity profiles. However, an unwanted side effect of this modification produced, as will be shown, a fictitious pressure gradient across the boundary layer that in turn caused substantial artificial convection. To see this, let's again consider the split flux G'_+, but now determined from eqn (5).

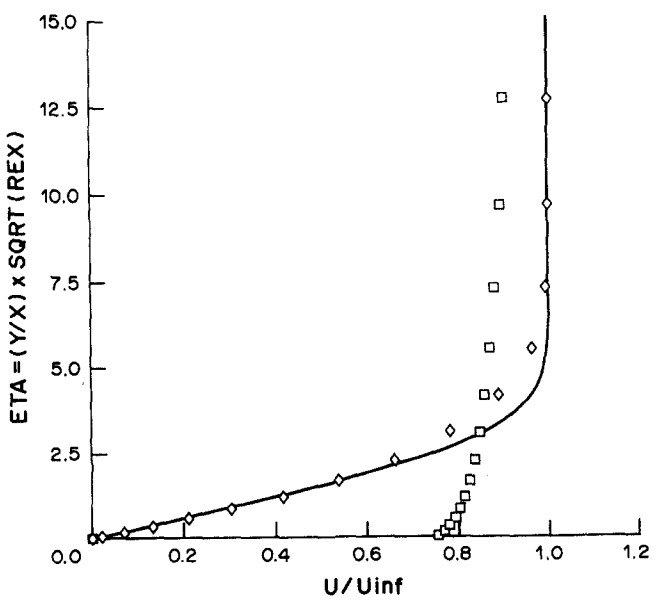

Fig. 3. Boundary layer velocity profiles. ◇ Modified solution; □ Steger–warming solution; — Blasius solution.

$$G'_+ = B_{+_{i,j+1/2}} U_{i,j} = \{S^{-1}R^{-1}C^{-1}\Lambda_+ CRS\}_{i,j+1/2} U_{i,j}$$

$$= \{S^{-1}R^{-1}C^{-1}\Lambda_+ CR\}_{i,j+1/2} \begin{bmatrix} 1 & 0 & 0 & 0 \\ -u/\rho & 1/\rho & 0 & 0 \\ -v/\rho & 0 & 1/\rho & 0 \\ \alpha\beta & -u\beta & -v\beta & \beta \end{bmatrix}_{i,j+1/2} \begin{bmatrix} \rho \\ \rho u \\ \rho v \\ e \end{bmatrix}_{i,j}$$

$$= \{S^{-1}R^{-1}C^{-1}\Lambda_+ CR\}_{i,j+1/2} \begin{bmatrix} \cdot \\ \cdot \\ \cdot \\ p' \end{bmatrix}_{i,j}$$

where:

$$p' = \beta[\alpha_{i,j+1/2}\rho_{i,j} - u_{i,j+1/2}(\rho u)_{i,j} - v_{i,j+1/2}(\rho v)_{i,j} + e_{i,j}]$$

$$= p_{i,j} + \frac{\beta}{2}\rho_{i,j}[(u_{i,j+1/2} - u_{i,j})^2 + (v_{i,j+1/2} - v_{i,j})^2].$$

Thus, in addition to the pressure, as was found earlier for the Steger–Warming form of flux splitting of eqn (4) (see the evaluation for G_+ given previously), we find a new term, always positive, that depends on the velocity gradient. Although this term is of the order Δy^2, it can produce a fictitious stress that can accelerate the fluid within the boundary layer and thereby create an unacceptably large artificial convection. This second order effect was caused by modifying the indices of the split Jacobian matrices from those originally given by Steger and Warming. Thus, either excess numerical diffusion results if the indices of the split flux Jacobians are chosen to match those on the U vector they multiply, or a fictitious pressure gradient causing an artificial convection results if they are chosen to match each other. To remove this adverse second order side effect, the split Jacobians were further modified within the boundary layer as follows:

$$\left.\begin{aligned} B'_{+_{i,j+1/2}} &= S^{-1}_{i,j_+}\{R^{-1}C^{-1}\Lambda_+ CR\}_{i,j+1/2} S_{i,j_+} \\ \text{and} \qquad & \\ B'_{-_{i,j+1/2}} &= S^{-1}_{i,j_-}\{R^{-1}C^{-1}\Lambda_- CR\}_{i,j+1/2} S_{i,j_-}, \text{ etc,} \end{aligned}\right\} \tag{7}$$

where $j + 1/2$ is defined as before, and

$$S_{i,j_+} = \begin{bmatrix} 1 & 0 & 0 & 0 \\ -(u/\rho)_{i,j+1/2} & (1/\rho)_{i,j+1/2} & 0 & 0 \\ -(v/\rho)_{i,j+1/2} & 0 & (1/\rho)_{i,j+1/2} & 0 \\ \alpha_{i,j}\beta & -u_{i,j}\beta & -v_{i,j}\beta & \beta \end{bmatrix},$$

and

$$S_{i,j_-} = \begin{bmatrix} 1 & 0 & 0 & 0 \\ -(u/\rho)_{i,j+1/2} & (1/\rho)_{i,j+1/2} & 0 & 0 \\ -(v/\rho)_{i,j+1/2} & 0 & (1/\rho)_{i,j+1/2} & 0 \\ \alpha_{i,j+1}\beta & -u_{i,j+1}\beta & -v_{i,j+1}\beta & \beta \end{bmatrix}.$$

Thus, only the fourth row of the S matrix (and consequently also the affected elements of S^{-1}) are changed back to the Steger–Warming formulation. All the rest remain as defined by eqn (6).

Figures 4(a) and (b) compare the velocity profiles calculated with the modified flux split method, with and without the pressure gradient correction, with the Blasius solution. Of particular note is the agreement of the corrected procedure profile in the magnified near wall region shown in Fig. 4(b). It is almost coincident with the Blasius solution. The difference in skin friction is approximately 0.6%. The remaining discrepancy shown near the knee of the profile in Fig. 4(a) is caused perhaps by the coarseness of the mesh or by the first order accuracy of the method.

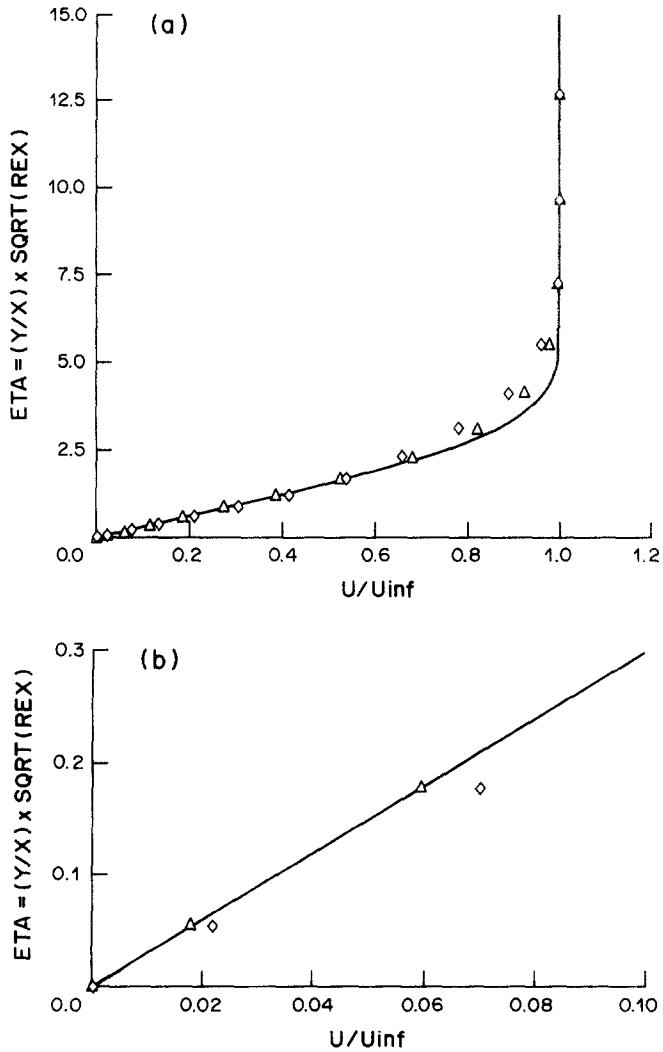

Fig. 4. (a) Velocity profiles using modified methods. (b) Velocity profiles in near wall region. ◇ Modified solution; △ modified solution with pressure gradient correction; — Blasius solution.

TURBULENT SUPERSONIC FLOW

An implicit flux split method, with the split Jacobians defined as in eqn (7) and the split fluxes defined by eqn (6) (except that the time index n was replaced by $n + 1$) was applied to solve for turbulent supersonic flow past a cone. In addition, the flux splitting was second order accurate outside the boundary layer. The viscous terms were also treated implicitly with second order accuracy everywhere. The resulting difference equations were solved in unfactored form by Gauss–Seidel line relaxation. References [2, 3] provide a description of the solution technique.

Figure 5 shows a 36×44 mesh about a cone of half angle 10° with approximately 20 points distributed through the boundary layer region. The freestream conditions correspond to Mach 6 flow at an altitude of 90,000 feet ($p = 36.144$ lbf/ft^2, $T = 403.3^\circ$ R, and Reynolds number of 10^6/ft).

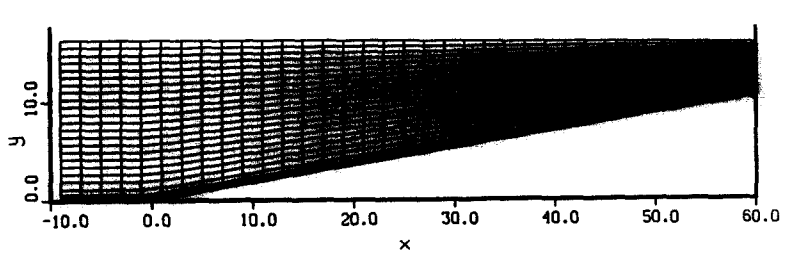

Fig. 5. Computational mesh about a cone.

The surface temperature of the cone was 1200° R and the boundary layer was tripped at $x = 5$ ft, measured from the point of the cone. At the edge of the boundary layer the tangential velocity $u_e' = 5.75 \times 10^3$ ft/s and the temperature $T_e = 552.5°$ R. This case was chosen to examine the quality of heat transfer predictions for a flow field of current engineering interest using flux split procedures on a computational mesh of common practice dimensions. The Reynolds averaged Navier–Stokes equations together with the Baldwin–Lomax turbulence model [12] were used to describe the flow. The numerical solution converged in approximately 80 time steps with the CFL number increasing from 10 to 2×10^8 during the course of the calculation. Figures 6(a) and (b) compare the calculated velocity profile at $x = 50$ ft with a boundary layer solution of Adams [13, 14]. The boundary layer solution contained 161 points across the boundary layer and for the purposes of this comparison is considered to be exact. Only some of the boundary layer solution points are shown in the figures. The agreement is fairly good and the skin friction is different by approximately 5% as shown in the magnified wall region in Fig. 6(b). Temperature profiles are compared in Figs 7(a) and (b) at

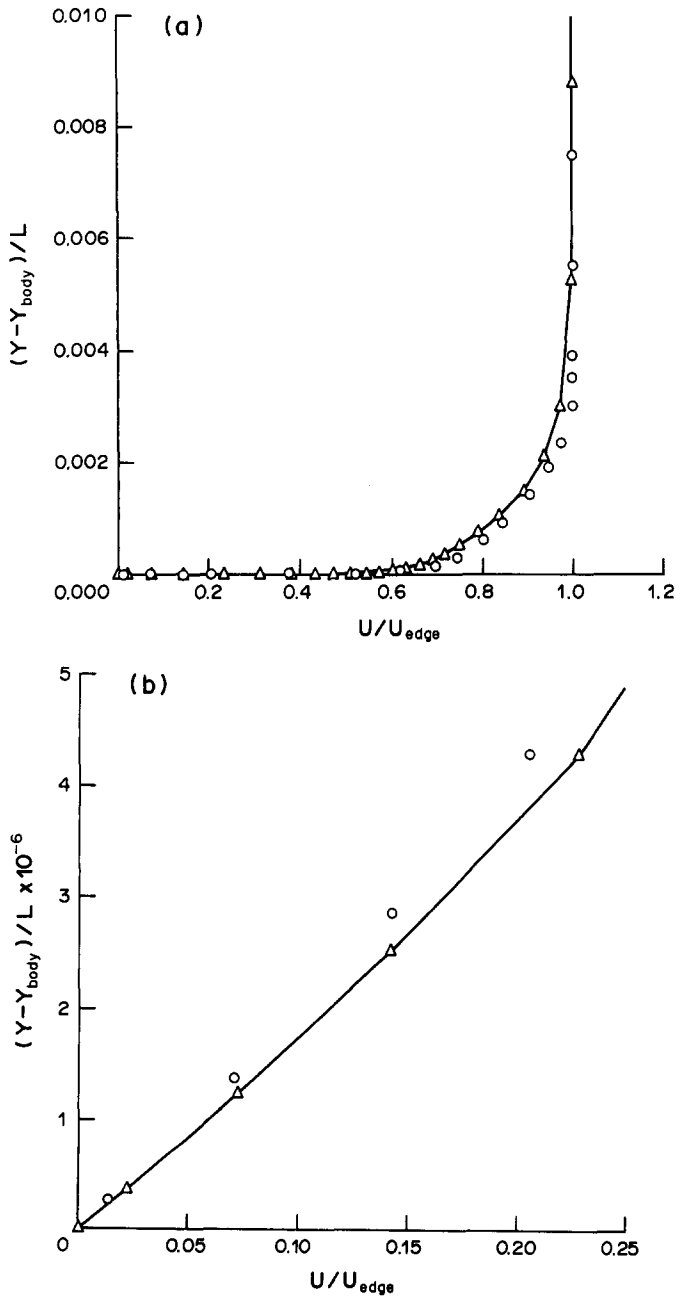

Fig. 6. (a) Velocity profiles on cone at $x = 50$ ft. (b) Velocity profiles near cone surface. —△— Present solution; ○ boundary layer solution—Adams.

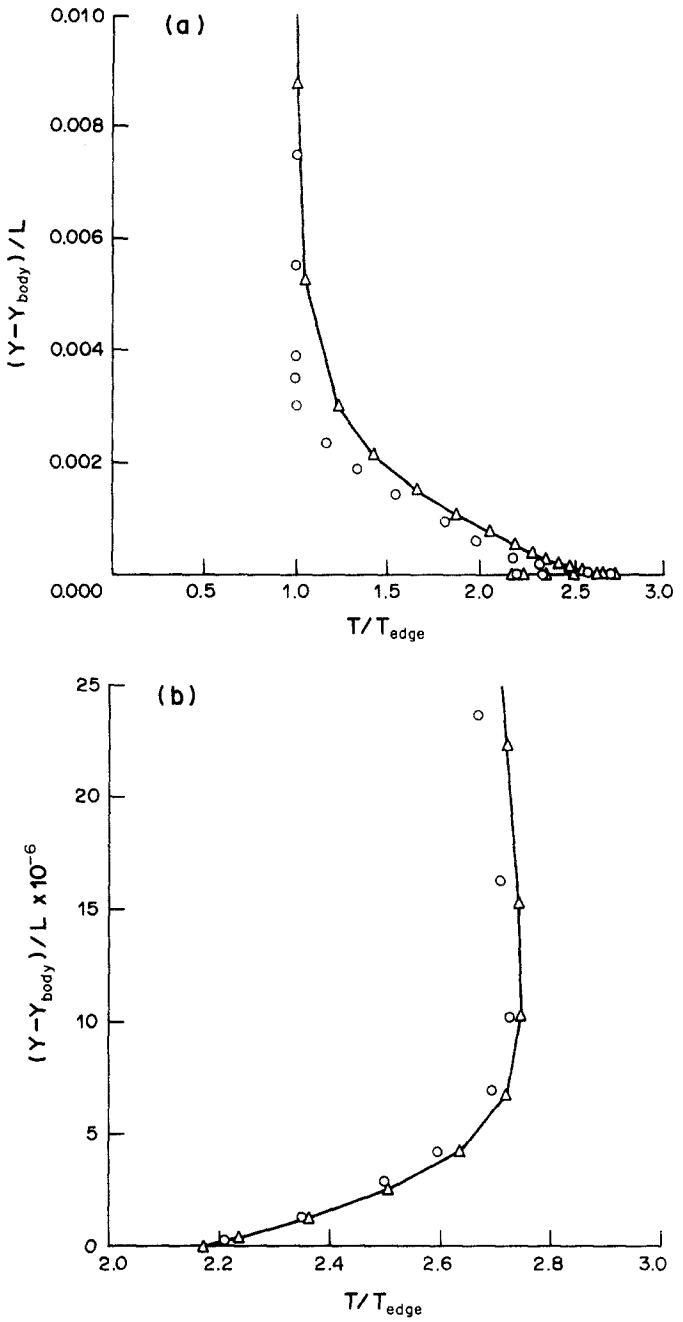

Fig. 7. (a) Temperature profiles on cone at $x = 50$ ft. (b) Temperature profiles near cone surface. —△— Present solution; ○ boundary layer solution—Adams.

the same location. Note the peak in temperature predicted very near the wall in Fig. 7(a). Figure 7(b) presents a magnified view of this region showing good agreement with the boundary layer solution for the gradient of temperature near the wall, and the value and location of its peak temperature. This good agreement could only be made if the turbulence models used in both calculations predicted the distribution and levels of turbulent eddy viscosity similarly. Adams used a Patankear–Spalding turbulence model [15] in his calculation. Figure 8 compares the eddy viscosity profiles of both calculations at $x = 50$ ft. As shown, the profiles are fairly similar with the largest differences occurring near the boundary layer edge.

The overall agreement of the present results with the boundary layer results of Adams is fairly good. However, there are some differences near the knees of the velocity profiles and in this same region for the temperature profiles. Some of this is probably caused by the differences in the turbulence models used. Other factors include comparing values at slightly different x–y locations

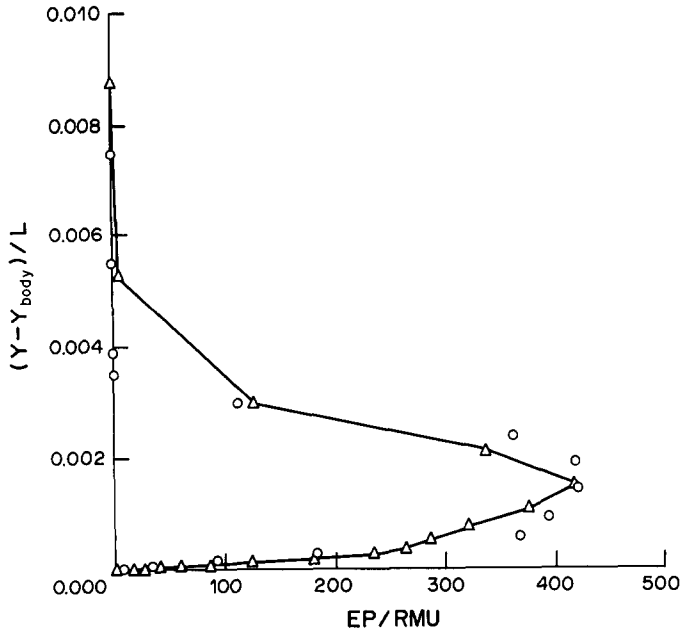

Fig. 8. Eddy viscosity profiles on cone at $x = 50$ ft. —△— Present solution; ○ boundary layer solution—Adams.

because the data for the boundary layer solution was given normal to the cone surface and those of the present calculation were at a constant x location, at most a 2% difference. The remaining difference represents numerical error from the computational method and coarseness of the mesh used in the present calculation.

HYPERSONIC FLOW

Gauss–Seidel line relaxation with flux splitting was also used to solve the equations describing the viscous flow of a chemically reacting gas in thermal nonequilibrium past a blunted cone at hypersonic speed [16]. Air (79% diatomic nitrogen and 21% diatomic oxygen) travelling at hypersonic speed through a standing shock wave will dissociate, forming atomic nitrogen and oxygen and creating nitric oxide. In addition, the vibrational temperatures of the diatomic molecules of the gas will be out of equilibrium temporarily with the translational and rotational temperatures following the sudden shocking of the gas. For such an axisymmetric flow, the set of equations required consists of 5 species continuity equations (N_2, O_2, NO, N and O), 2 momentum equations, 3 vibrational energy equations, and a total energy equation. An implicit block matrix formulation for the governing equations solves for both the flow equations and the gas chemistry and thermodynamics in a fully coupled manner. The block matrix elements are of dimension 11×11.

Figure 9 shows the mass concentrations for atomic oxygen about a sphere-cone body (cone half angle of 10.5°) in Mach 17.94 flow. The nose radius is 20 cm, constant wall temperature is 1500 K, and the freestream conditions correspond to an altitude of 50 km. Figures 10(a) and (b) show the contours of translational and vibrational temperature, respectively. Note the massive extent of thermal nonequilibrium occurring in the flow field. Figures 11(a) and (b) compare the reacting gas results for surface pressure and heat transfer with those for a perfect gas. The surface pressures agree well, but the reacting gas calculation shows considerably more heat transfer to the sphere-cone body. This is caused by the release of internal energy in the cool wall region by the recombination of atomic nitrogen and oxygen to form their respective diatomic molecules. Approximately 250 iterations and 7 min of CRAY XMP computer time were required to obtain converged solutions on a 30×30 mesh.

CONCLUSIONS

Gauss–Seidel line relaxation can be used to solve the Navier–Stokes equations efficiently. The convergence efficiency depends upon the weights of the diagonal matrix elements in the finite

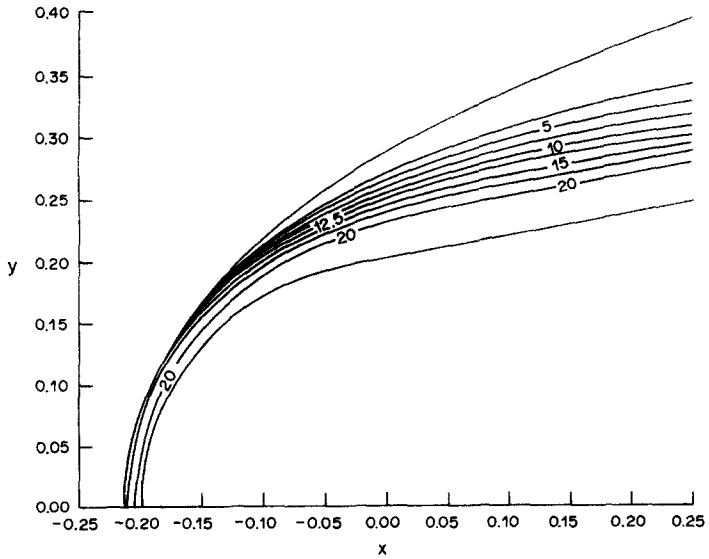

Fig. 9. Contours of mass concentration of atomic oxygen in percent.

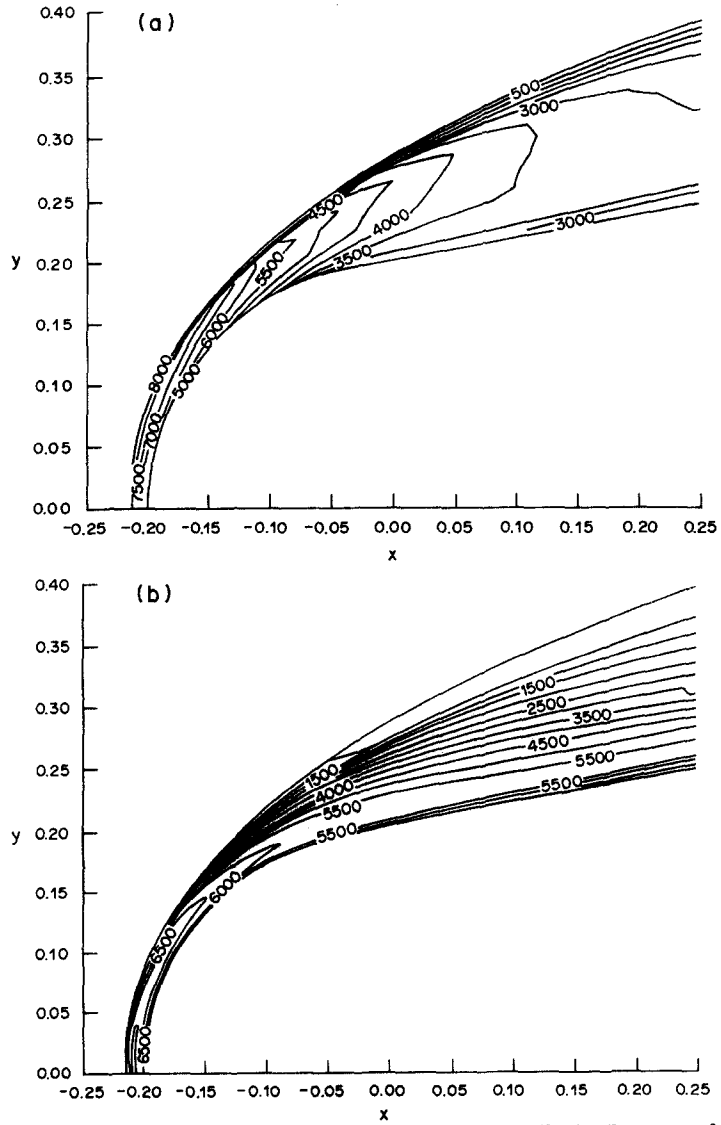

Fig. 10. (a) Contours of translational–rotational temperature in degrees K. (b) Contours of vibrational temperature in degrees K.

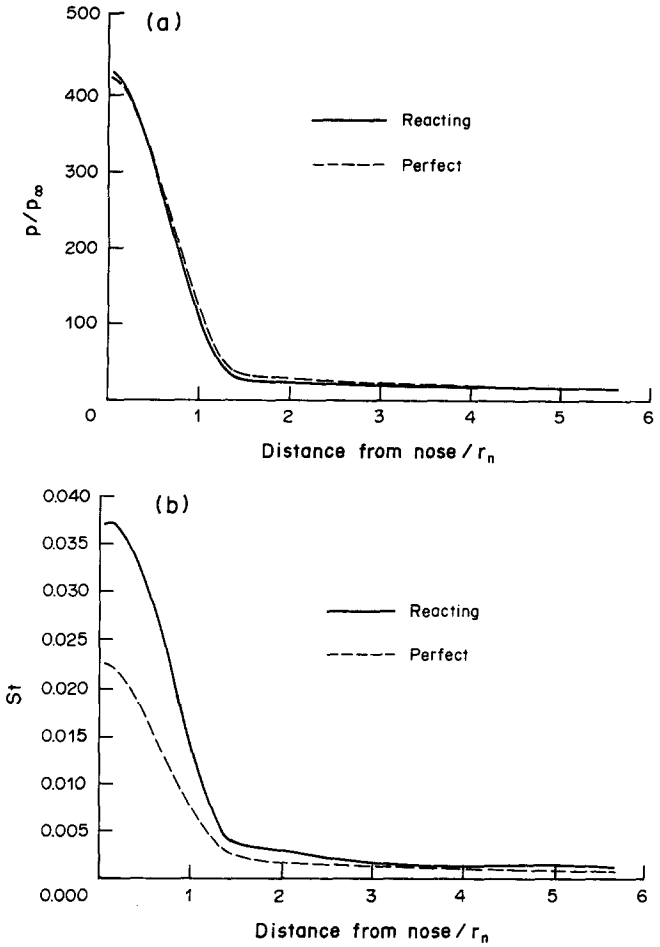

Fig. 11. (a) Surface pressure distribution for reacting and perfect gases. (b) Heat transfer distributions for reacting and perfect gases (St, Stanton number).

difference equations used to approximate the governing compressible viscous flow equations. Flux split difference approximations used to maximize diagonal element weight can adversely affect solution accuracy in viscous shear layer regions if not done carefully. Flux split procedures have been devised for accurate shear layer calculations.

Gauss–Seidel line relaxation with type dependent differencing, used previously to solve the Transonic Small Disturbance equation, the Full Potential equation, and the Euler equations, has been verified for solving the Navier–Stokes equations, and has been extended for solving the equations describing the viscous flow of a chemically reacting gas in thermal nonequilibrium at hypersonic speeds.

Acknowledgements—The authors would like to acknowledge the support for this work from the following sponsors. SDIO/IST managed by the Army Research Office under contract No. DAAL03-86-K-0139, the Department of the Air Force under contract No. F33615-86-C-3015, and NASA under a Hypersonic Training and Research Grant No. NAGW 965.

REFERENCES

1. J. L. Thomas and R. W. Walters, Upwind relaxation algorithms for the Navier–Stokes equations. AIAA Paper 85-1501 (1985).
2. R. W. MacCormack, Current status of numerical solutions of the Navier–Stokes equations. AIAA Paper 85-0032 (1985).
3. G. V. Candler and R. W. MacCormack, Hypersonic flow past 3-D configurations. AIAA Paper 87-0480 (1987).
4. R. W. Newsome, R. W. Walters and J. L. Thomas, An efficient iteration strategy for upwind/relaxation solutions to the thin layer Navier–Stokes equations. AIAA Paper 87-1113-CP (1987).
5. J. L. Steger and R. F. Warming, Flux vector splitting of the inviscid gasdynamic equations with application to finite difference methods. *J. Comput. Phys.* **40**, 263–293 (1981).
6. B. van Leer, J. L. Thomas, P. L. Roe and R. W. Newsome, A comparison of numerical flux formulas for the Euler and Navier–Stokes equations. AIAA Paper 87-1104-CP (1987).

7. W. G. Vincenti, C. B. Wagoner and N. H. Fisher Jr, Calculations of the flow over an inclined flat plate at free-stream Mach number 1. NACA Technical Note 3723 (1956).
8. E. M. Murman and J. D. Cole, Calculation of plane steady transonic flows. *AIAA J.* **9,** 114–121 (1971).
9. A. Jameson, Numerical calculation of the three-dimensional transonic flow over a yawed wing. *Proc. AIAA Comp. Fluid Dyn. Conf.*, Palm Springs (1973).
10. G. Moretti, Three-dimensional, supersonic, steady flows with any number of imbedded shocks. AIAA Paper 74-10 (1974).
11. S. R. Chakravarthy, Relaxation methods for unfactored implicit upwind schemes. AIAA Paper 84-0165 (1984).
12. B. S. Baldwin and H. Lomax, Thin layer approximation and algebraic model for separated flow. AIAA Paper 78-257 (1978).
13. J. C. Adams, Eddy viscosity-intermittency factor approach to numerical of transitional heating on sharp cones in hypersonic flow. AEDC-TR-70-210 (1970).
14. J. C. Adams, Implicit finite-difference analysis of compressible laminar, transitional, and turbulent boundary layers along the windward streamline of a sharp cone at incidence. AEDC-TR-71-235 (1971).
15. S. V. Patankar and D. B. Spalding, *Heat and Mass Transfer in Boundary Layers*. CRC Press, Cleveland, Ohio (1968).
16. G. V. Candler and R. W. MacCormack, The computation of hypersonic flows in chemical and thermal nonequilibrium. *Proc. Third National Aero-Space Plane Technology Symposium*, Paper No. 107 (1987).